Chapter 2
Tailoring of Soft Magnetic Properties and High Frequency Giant Magnetoimpedance in Amorphous Ribbons

L. González-Legarreta, V.M. Prida, A. Talaat, M. Ipatov, V. Zhukova, Arcady Zhukov, LI. Escoda, J.J. Suñol, J. González, and B. Hernando

2.1 Introduction

Among several industrial sectors nowadays demanding advanced soft magnetic materials such as magnetic sensors and actuators are one of the most active [1]. Amorphous soft magnetic thin films, microwires, and ribbons present excellent magnetic properties not only interesting from the basic point of view but also suitable for technological applications [2]. In the absence of magneto-crystalline anisotropy the magnetoelastic anisotropy of amorphous materials is the main factor determining their magnetic properties. This magnetoelastic anisotropy, K_{me}, given by the equation: $K_{me} \sim 3/2\lambda_s\sigma_i$, is affected by internal stresses, σ_i, and magnetostriction coefficient, λ_s, is the saturation magnetostriction [3]. Giant magnetoimpedance, GMI, is one of the most promising effects for technical applications [1, 4, 5] being proposed for several magnetic sensor applications [6, 7]. Rapidly solidified Co-based alloys displaying nearly zero magnetostriction

L. González-Legarreta • V.M. Prida • B. Hernando (✉)
Department of Physics, University of Oviedo, Ave. Calvo Sotelo s/n, 33007 Oviedo, Spain
e-mail: grande@uniovi.es

A. Talaat • M. Ipatov • V. Zhukova • J. González
Department of Materials Physics, University of the Basque Country, Paseo Manuel de Lardizábal 3, 20018 San Sebastián, Spain

A. Zhukov
Department of Materials Physics, Basque Country University, UPV/EHU, San Sebastian 20018, Spain

Departamento de Física Aplicada, EUPDS, Basque Country University, UPV/EHU, San Sebastian 20018, Spain

IKERBASQUE, Basque Foundation for Science, Bilbao, Spain

L. Escoda • J.J. Suñol
Girona University, Campus Montilivi, ed. PII, Lluís Santaló s/n, 17003 Girona, Spain

A. Zhukov (ed.), *High Performance Soft Magnetic Materials*, Springer Series in Materials Science 252, DOI 10.1007/978-3-319-49707-5_2

exhibit soft magnetic properties that may be enhanced by controlled annealing treatment [8–12]. From the perspective of highly sensitive magnetic sensor and in order to achieve a suitable GMI response, we have investigated the effects of stress and current annealing on magnetic and magnetoimpedance properties of near-zero magnetostriction of $Co_{66.3}Fe_{3.7}Si_{12.0}B_{18.0}$ and $Co_{71.25}Fe_{3.75}Si_{10}B_{15}$ amorphous alloy ribbons.

2.2 Giant Magnetoimpedance Effect

The so-called giant magnetoimpedance (GMI) effect is the large change in the ac impedance of a soft ferromagnetic conductor induced by a dc magnetic field [13, 14]. This change is usually defined by the GMI ratio as:

$$\Delta Z/Z(\%) = 100\% \times \frac{Z\,(H) - Z\,(H_{\max})}{Z\,(H_{\max})} \tag{2.1}$$

where $Z(H)$ and $Z(H_{\max})$ represent the impedance in an applied field H and in an external magnetic field sufficient to saturate magnetically the sample, respectively. In practice, the value of $H_{\max}$ is the maximum field available for the experimental equipment.

GMI effect can be explained by means of Maxwell equations of electrodynamics together with the Landau–Lifshitz–Gilbert equation of the magnetization dynamics [15]. Analytically, it is difficult to obtain the exact solution of the problem by solving simultaneously these equations. However, at low-intermediate frequencies the problem can be treated with a quasi-static approximation. In this case, assuming the material relationship between the induction and magnetic field is linear, $B = \mu H$, the diagonal and off-diagonal components of the impedance tensor [16] for an infinite planar film with thickness, d, are [17]:

$$Z_{zz} = R_{dc}\xi \cot \xi \tag{2.2}$$

$$Z_{yz} = -i\omega\mu_{zy}\frac{(1 - \cos \xi)}{(2\xi \sin \xi)} \tag{2.3}$$

where R_{dc} is the dc electrical resistance, $\xi = (1 - i)\delta/(2d)$, and δ is the penetration depth in a magnetic medium,

$$\delta = \sqrt{2\rho/\omega\mu_{yy}} \tag{2.4}$$

where ρ is the electrical resistivity and $\omega = 2\pi f$ is the angular frequency of the driving ac current. The components of permeability tensor are $\mu_{yy} = \mu_0(1 + \cos^2 \theta\chi_t)$ and $\mu_{zy} = -\mu_0 \sin\theta\cos\theta\chi_t$, where θ is the angle between the total magnetic field H and the magnetization M of the sample, and the transverse susceptibility χ_t is

obtained by solving Landau–Lifshitz–Gilbert equation [15]. When $I_{dc} = 0$, the component of permeability μ_{yy} is constant.

At high frequencies, $f \sim$ GHz, the quasi-static approximation is no longer applied and ferromagnetic resonance (FMR) takes place. Therefore, the nonlinearity of Landau–Lifshitz equation must be taken into account, since nonlinear effects should appear [18]. A complete GMI description including dynamical effects with different degrees of approximations has been reported by several authors [15, 19]. In this frequency range, the resonance frequencies satisfy the Kittel resonance condition for a thin film magnetized along the in-plane uniaxial easy axis [18, 20]:

$$f^2 = \left(\gamma^2 {\mu_0}^2 / 4\pi^2\right) \left[\left(H + H_K\right)\left(H + H_K + M_S\right)\right] \tag{2.5}$$

where γ is the gyromagnetic ratio of the electron, H_K the anisotropy field, and M_S the respective saturation magnetization. γ is expressed as:

$$\gamma = g \frac{\mu_0 e}{2m_e} \tag{2.6}$$

where m_e and e are the mass and charge of the electron, respectively, and g is the Landé splitting factor.

As have been mentioned above, GMI depends on the frequency of the ac driving current, which flows through the sample, being possible classify the effect into four frequency regimes.

1. *Very low frequencies* ($f \sim 10$ kHz): the skin effect is rather weak. This is due to the skin depth at these frequencies that is usually larger than the thickness of the sample. The principal contribution to the transverse magnetic permeability (μ_t) and hence to the GMI effect comes from the inductive voltage. It is called magnetoinductive effect.
2. *Low frequencies* ($f \sim 10$ MHz): the skin effect is strong and changes of the transverse magnetic permeability and hence to the GMI are caused by domain walls movement and magnetization rotation.
3. *Intermediate frequencies* ($f \sim 1000$ MHz): the GMI effect is also originated by the skin effect. However, at these frequencies the domain walls are strongly damped. Thus the magnetization rotation must be considered as responsible for the transverse magnetic permeability change induced by the external magnetic field [14].
4. *High frequencies* ($f \sim$ GHz): the magnetization rotation is strongly influenced by the gyromagnetic effect and ferromagnetic relaxation. At this frequency range, strong changes of the sample impedance are attributed to the ferromagnetic resonance (FMR) [14].

2.3 Amorphous Ribbons Production

Soft ferromagnetic amorphous ribbons were produced by melt spinning at cooling rates of 10^3–10^6 K/s. This technique avoids prolonged conventional annealing stages. Complementary heat treatments of ribbons as stress annealing or current annealing will be discussed in Sect. 2.4.3.

2.3.1 Melt Spinning

Melt spinning process is often performed by rapid cooling of a bulk master alloy. This primary alloy can be prepared from high purity elements by arc melting under Ar atmosphere. Samples should be remelted several times to assure alloy compositional homogeneity [21]. Amorphous Co- or Fe-rich soft ferromagnetic amorphous alloys are produced by rapid quenching from the melt in vacuum or in inert atmosphere. Figure 2.1 shows a schema (*left*) of the melt spinning procedure. The as-prepared ribbons can be annealed in a vacuum chamber or in a furnace. It is known that annealing can modify the structure and MI response of the amorphous soft ferromagnetic materials through: (a) the structural relaxation and stress release of the amorphous phase [22], (b) the growth of a crystallized layer at the sample surface [23], or (c) the nanocrystallization in the bulk material [24]. In the literature, many annealing temperature and times were applied [24, 25]. Furthermore, it is possible to anneal ribbons by laser or by microwave [26]. One option to improve magnetic anisotropy during the quenching production is two apply a magnetic field during the fabrication process (field-quenched sample) [27].

After annealing, the samples were cooled in furnace until the chamber temperature is near room temperature or rapidly quenched in water or ice. Cooling is usually performed under vacuum (at a low partial pressure to the order of 10^{-3}

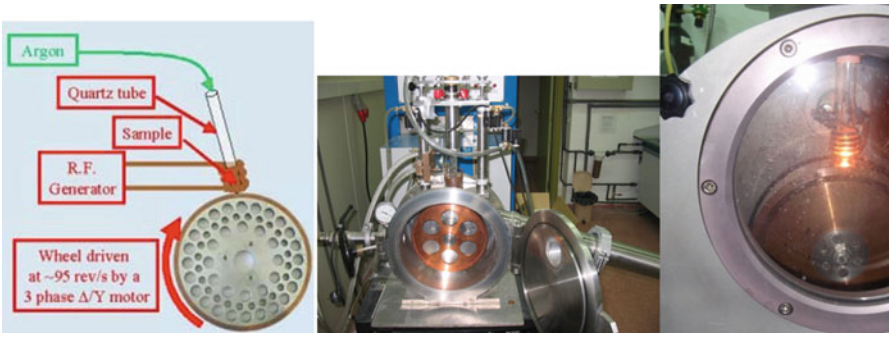

Fig. 2.1 Experimental melt spinning equipment and schema of the melt spinning process

Torr) or under inert atmosphere. Sometimes samples were annealed in air to develop an oxide coating on the surface and to evaluate the effect of the oxide [28]. The structure of the annealed samples remains amorphous or is nanocrystalline. Concerning nanocrystallization, one of the problems is that it renders these alloys extremely brittle limiting their practical application [29].

2.3.2 *Structural Characterization*

In order to get confirmation of the amorphous microstructure of the alloy, X-ray or neutron diffraction measurements were performed at room temperature. Figure 2.2 shows the amorphous X-ray diffraction patterns of three Co-rich ribbons produced by melt spinning. The as-quenched samples presented a broad hump, which is characteristic of the amorphous phase.

The existence of the amorphous phase can also be checked by high-resolution transmission microscopy (HRTEM) [30]. Furthermore, transmission Mössbauer spectroscopy (TMS) is useful in Fe-rich samples [31]. Figure 2.3 shows a micrograph (obtained by scanning electron microscopy, SEM) of the wheel surface of a ribbon flake (*left*) and a typical HRTEM amorphous halo (*right*).

In order to check thermal stability of the amorphous phase against crystallization thermal analysis experiments are usually performed. As an example, Fig. 2.4 shows the differential scanning calorimetry (DSC) heating scans of two amorphous ribbons [27].

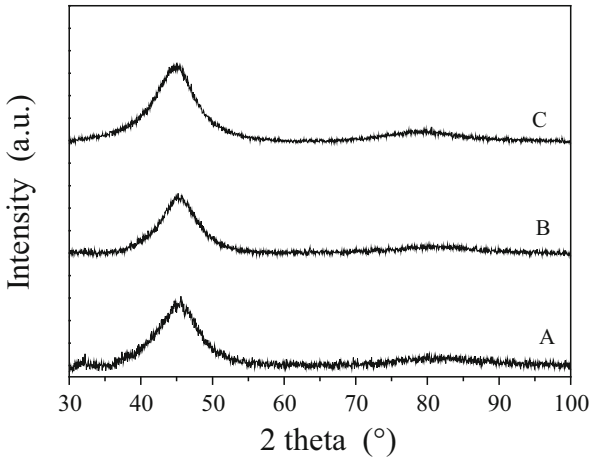

Fig. 2.2 X-ray diffraction patterns at room temperature of three Co-rich amorphous ribbons produced by melt spinning

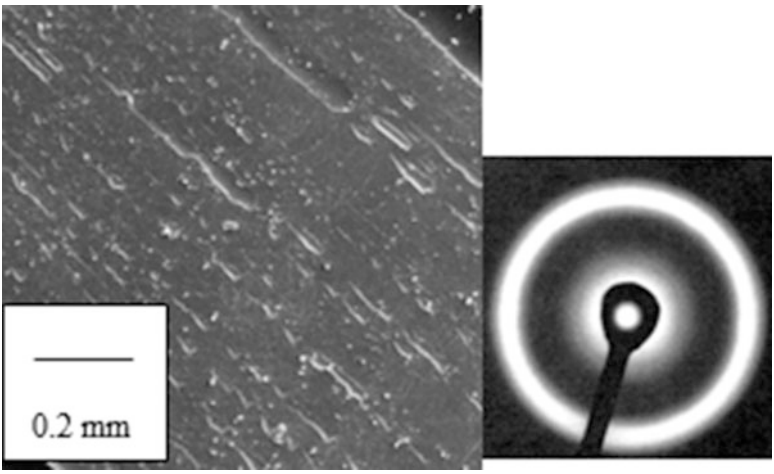

Fig. 2.3 SEM micrograph of the wheel surface of a ribbon (*left*) and an HRTEM amorphous halo (*right*)

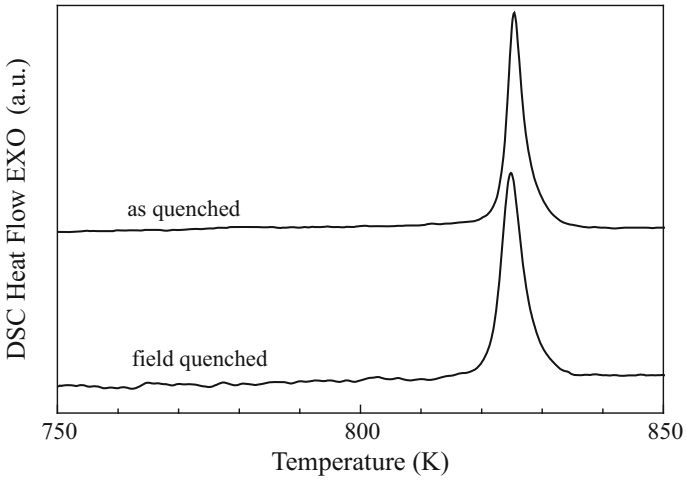

Fig. 2.4 DSC heating scans of two amorphous soft ferromagnetic ribbons produced by melt spinning: conventional quenching (*up*), quenching under magnetic field (*down*)

2.4 Experimental Techniques

2.4.1 Magnetic Characterization: Hysteresis Loops and Magnetostriction

Hysteresis loops for all ribbons were measured along the ribbon axis at a frequency value of 50 Hz using the conventional induction technique. Isothermal $M(H)$ loops at room temperature for the three stress-annealed $Co_{66.3}Fe_{3.7}Si_{12.0}B_{15.0}$ samples

show an almost ideal behavior, with a constant slope nearly up to saturation and a quasi-absence of hysteresis effect. All samples exhibit an induced anisotropy perpendicular to the ribbon axis, and a saturation magnetization, $\mu_0 M_S$, of 0.53 T. Sample 1 has the smallest effective anisotropy field of 360 A/m, while the effective anisotropy fields of 530 A/m and 550 A/m were determined for samples 2 and 3, respectively. The anisotropy fields were estimated with an accuracy of the 0.5 % in all cases [32]. Magnetostriction coefficients were obtained by the small angle magnetization rotation (SAMR) technique [33].

2.4.2 Measurement of GMI Effect

The set-up in this work used to measure the giant magnetoimpedance of Co-based amorphous ribbons is shown in Fig. 2.5.

Impedance components measurements were carried out on the as-quenched and annealed Co-based 1 cm long ribbons soldered to a specially designed micro-strip sample holder. The sample holder is placed inside a long solenoid, which generates a homogenous magnetic field H_E up to 20 kA/m along the ribbon axis. In addition, this system allows the application of a transversal bias field H_B created by dc bias current I_b applied to the sample by a bias-tee element. This system is connected to a vector network analyzer N5230A (VNA), which allows measuring simultaneously the longitudinal and off-diagonal impedance component of the sample in the frequency range of 100–3500 MHz [34]. The longitudinal impedance component is obtained from the reflection coefficient S_{11} by:

$$Z_{zz} = Z_0 \frac{(1 + S_{11})}{(1 - S_{11})} \tag{2.7}$$

where $Z_0 = 50\ \Omega$ is the characteristic impedance of the electric coaxial line. The off-diagonal impedance Z_{yz} component is measured through the transmission coefficient S_{21} as a voltage induced in a 2 mm long pick-up coil wound around the ribbon sample (see Fig. 2.5).

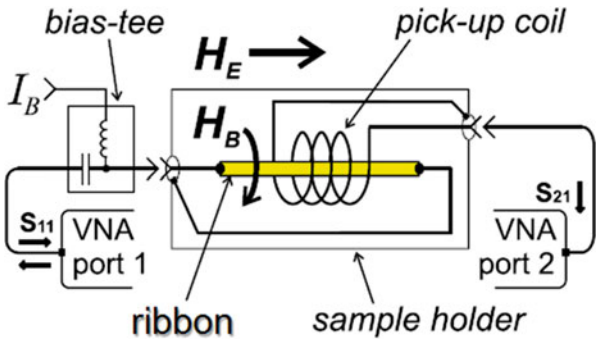

Fig. 2.5 Experimental set-up for measuring the GMI response of Co-based ribbons

The analyzer power output in all measurements presented here was 10 dBm that corresponds to a 1.4 mA high frequency driving current passing through the ribbon.

2.4.3 Thermal Treatments: Stress Annealing and Current Annealing

One of the most interesting aspects concerning to the research to get a larger GMI effect is the reduction of the skin effect by choosing magnetic materials with large permeability and small skin depth [19]. For the last purpose we need that the transverse component (in the case of ribbons) of the magnetic susceptibility to be very sensitive to the external magnetic field in order to the skin depth effect can be modified by the action of the magnetic field reflecting in strong changes of the electrical impedance owing the variation of the effective cross section to the electrical transport. These modifications of the transverse component of the magnetic susceptibility can be reached by submitting the amorphous ribbons to thermal treatment under the action of a stress and/or magnetic field, which can develop a uniaxial magnetic anisotropy with the magnetization easy axis transverse to the longitudinal direction of the ribbon [35, 36].

In this work, the studied $Co_{66.3}Fe_{3.7}Si_{12.0}B_{18.0}$ and $Co_{71.25}Fe_{3.75}Si_{10}B_{15}$ amorphous alloy ribbons present transverse induced magnetic anisotropy by stress and current annealing, respectively.

For $Co_{66.3}Fe_{3.7}Si_{12.0}B_{18.0}$ ribbon, which exhibits in the as-quenched state a saturation magnetostriction at room temperature of the order of $\lambda_S \sim -0.18 \times 10^{-6}$, we took three pieces, which were submitted to the following stress-annealing treatment:

1. Sample 1: tensile stress annealing at 400 °C with 300 MPa during 1 h, without pre-annealing.
2. Sample 2: pre-annealing at 340 °C during 1 h, followed by a tensile stress annealing at 340 °C with 300 MPa during 1 h.
3. Sample 3: pre-annealing at 360 °C during 1 h, followed by a tensile stress annealing at 360 °C with 300 MPa during 1 h.

In all thermal treatments the tensile stress was applied along the ribbon axis. After annealing, these samples changed the magnetostriction coefficient to $+0.04 \times 10^{-6}$, $+0.17 \times 10^{-6}$, and $+0.11 \times 10^{-6}$, respectively.

For $Co_{71.25}Fe_{3.75}Si_{10}B_{15}$ amorphous ribbon, which exhibits in the as-quenched state a saturation magnetostriction at room temperature of the order of $\lambda_S \sim -6 \times 10^{-7}$, we took different pieces which were submitted to current annealing [37], i.e., a dc electrical current (440–680 mA) was passing along the ribbon during 5 min. An estimation of the temperature produced by the annealing can be obtained from [35] and Fig. 2.2. Then, for the current intensity range here employed that the averaged temperature within the sample was ranging in (274–427 °C), being something lower at

dc borders of the ribbon because of dissipative effects. Besides, the dc current flowing along the ribbon generates a maximal transverse magnetic field from 6.9×10^3 A/m up to 10.6×10^3 A/m.

These thermal treatments develop a macroscopic uniaxial magnetic anisotropy that will play a drastic role regarding the giant magnetoimpedance effect of these treated ribbons.

2.5 Results and Discussion

Here it will be presented the results of the magnetoimpedance response of near-zero magnetostriction of $Co_{71.25}Fe_{3.75}Si_{10}B_{15}$ and $Co_{66.3}Fe_{3.7}Si_{12.0}B_{18.0}$ amorphous ribbons exhibiting a macroscopic uniaxial magnetic anisotropy induced by current annealing (440–680 mA during 5 min) in the first ribbon and by stress-annealing treatment (300 MPa applied tensile stress at different temperature, i.e., 340, 360, and 400 °C, during 1 h) in the second one, in the frequency range from 100 MHz up to 3500 MHz.

2.5.1 Induced Anisotropy Influence on GMI Components in Stress-Annealed Co-Based Amorphous Ribbons

To explore the effect of induced anisotropy by stress annealing on GMI components of $Co_{66.3}Fe_{3.7}Si_{12.0}B_{18.0}$ amorphous alloy ribbon, we have submitted to some pieces of the ribbon at three different treatments, aforementioned.

Firstly, we have studied the diagonal impedance for the three ribbons in the frequency range of 100–3500 MHz. The absolute value of the longitudinal impedance, Z_{zz}, measured as a function of the applied field for selected values of the frequency for the three samples is shown in Fig. 2.6. It can be observed that for the sample 1 (Fig. 2.6a), which does not have been submitted to any pre-annealing, the impedance evolves to a symmetric two-peaks behavior with respect to H as the frequency increases. Meanwhile, the impedance behavior for samples 2 and 3 (Fig. 2.6b, c, respectively), which have been submitted to a stress relaxation followed by stress annealing at different temperatures, displays different features. The GMI response shows a not enough well-defined two-peaks pattern at low frequencies below 150 MHz for sample 2, but above this frequency a two-peaks pattern emerges clearly. Meanwhile, sample 3 displays an asymmetric two-peaks behavior below 150 MHz, which vanishes as the frequency increases. The different features observed in these annealed ribbons can be explained by the influence of the respective anisotropy induced by each performed annealing under tensile stress on their susceptibility. The two-peaks behavior is more defined and the GMI effect displays its maximum value for sample 1 annealed at 400 °C without previous stress

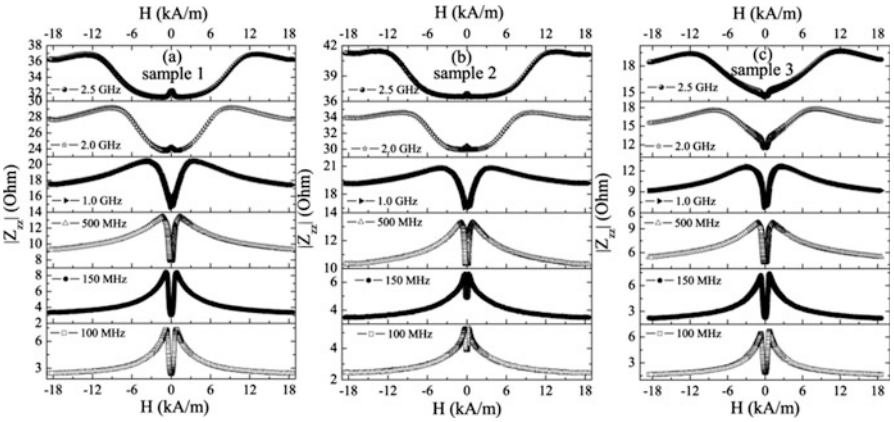

Fig. 2.6 Magnetic field dependence of diagonal impedance component at selected frequencies for stress-annealed $Co_{66.3}Fe_{3.7}Si_{12.0}B_{18.0}$ samples

relaxation, indicating the optimum conditions for induced anisotropy and lower magnetostriction coefficient in comparison with the other two annealed samples. Higher anisotropy fields are detected in stress-annealed samples 2 and 3 as a consequence of the smaller magnitude of the non-recoverable plastic contribution to the induced anisotropy arising from the pre-annealing. Furthermore, the asymmetric character of the GMI in sample 3 could be attributed to the partial crystallization taken place at the surface of this ribbon annealed at 360 °C during 2 h, as a consequence of the different anelastic contribution to the stress-induced anisotropy in the crystallized surface of this sample in comparison with the other two annealed ribbons [32].

Concerning the frequency dependence with the field corresponding to the Z_{zz} maximum, it is observed that the MI peaks are shifted to higher magnetic fields as the frequency is raised. This shift is related to the variation of the skin depth with the frequency-dependent magnetic permeability. In fact, the presence of stress-induced anisotropy with the easy magnetization direction perpendicular to the ribbon axis leads to significantly high values of the transverse magnetic permeability for these samples. In addition, this shift results an evidence of the ferromagnetic resonance contribution to the impedance [38]. Studying the position of the FMR peaks, i.e., the frequency at which appears a maximum of the impedance for each applied field, the data can be fitted by the well-known FMR expression described above (Eq. (2.5)). The results for the three samples are displayed in Fig. 2.7.

It shows a good agreement between the fitting of the resonance frequencies and the Kittel resonance condition (Eq. (2.5)). The experimental results provide us the anisotropy effective fields of $H_K = 290$ A/m for sample 1, $H_K = 550$ A/m for sample 2, and $H_K = 650$ A/m for sample 3. These values are comparable to derived ones from hysteresis loops measured along the ribbon axis at 50 Hz [32].

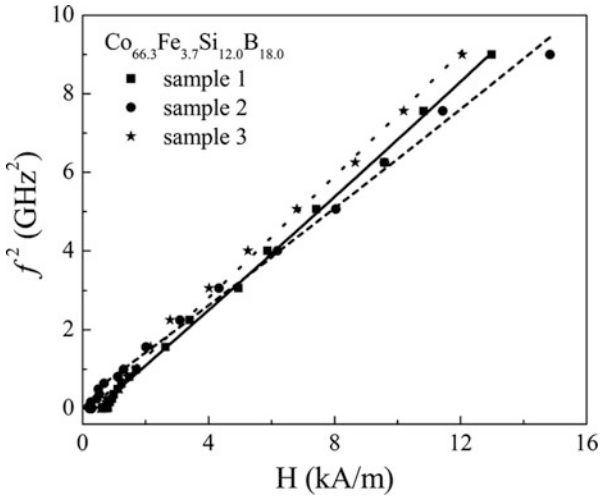

Fig. 2.7 Square of resonance frequency as a function of the resonance field for the three annealed ribbons. Symbols denote experimental data and lines denote theoretical fits by Eq. (2.5)

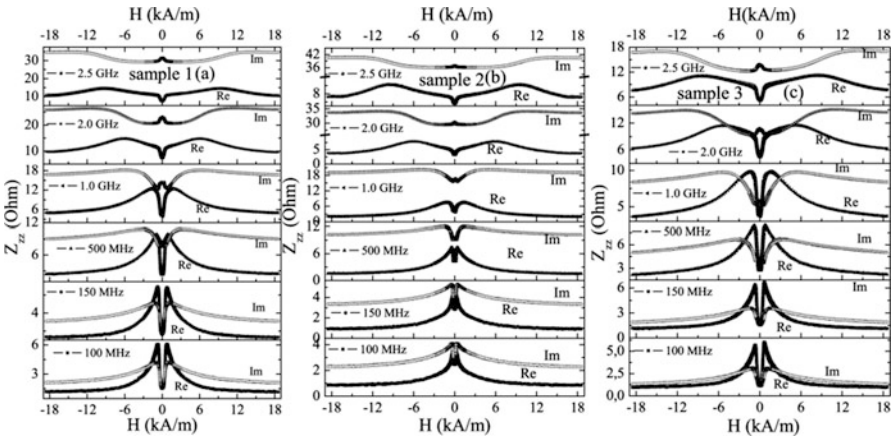

Fig. 2.8 Real (R) and imaginary (χ) parts of the impedance as a function of the applied magnetic field for several frequencies for the three stress-annealed samples

The effect of FMR is even more evident when the field dependence of real (R) and imaginary (X) part of diagonal impedance is plotted. In Fig. 2.8, it can be observed that at low frequency (below 500 MHz), the R and X impedance components show a parallel trend. However, at high frequency, when the maximum in the real part occurs then a slope change in the imaginary part vs. applied field is displayed, according to the characteristic behavior of the imaginary impedance component at resonance [38].

We have also explored the off-diagonal impedance component for these three ribbons. The off-diagonal GMI is a cross-magnetization process that is due to the appearance of a longitudinal magnetization when the sample is transverse

magnetized by the excitation current pass through it, i.e., a non-zero off-diagonal component of the permeability tensor is present in the ferromagnetic conductor [39, 40].

The reactance of the pick-up coil for $S_{21}(H)$ detection starts to affect the measurements as the frequency increases, therefore we present the off-diagonal measurements at lower frequencies than the longitudinal ones. Figure 2.9 shows the real part of off-diagonal impedance $Z_{yz}(H) \sim S_{21}(H)$ measured at 100 MHz with different dc bias currents I_b for all samples. The amplitude of bias current I_b was small to prevent the ribbon overheating and crystallization. For $I_b = 0$, the off-diagonal impedance shows symmetric peaks for applied field values in the vicinity of the anisotropy field $\pm H_K$, for each ribbon. In this case, the total response should be zero for all field range; however, these symmetric peaks are due to the small residual helical anisotropy, which remains in the samples after been submitted to stress annealing [41]. With $I_b = 50$ mA the off-diagonal response significantly increases and becomes antisymmetric with respect to the field H, having almost linear behavior in the field range of ± 500 A/m, for the three samples. This behavior can be explained as follows. The transverse dc field created by the bias current makes one or the opposite (depending on the current direction) transverse magnetization direction more favorable. Domains with magnetization lying along the bias field increase at the expense of domains with magnetization aligned against this field. If it is sufficiently large, domains with magnetization lying along the bias field collapse forming a single domain structure. Then, both the axial external magnetic field and the transverse dc bias field determine the re-magnetization process [42, 43]. Besides, if this field is sufficiently high, the field dependence of the off-diagonal impedance becomes asymmetric and anhysteretic [44] as it is shown in Fig. 2.9. The quasi-linear behavior near $H = 0$ of $Z_{yz}(H)$ is rather interesting for field sensors [17, 34, 44].

The frequency dependence of diagonal and off-diagonal impedance components is completely different. In Fig. 2.10 the maximum values of $|Z_{zz}|$ and S_{21} as a function of frequency are represented for the three samples. As can be observed in it the diagonal impedance component increases monotonously; however, the off-diagonal one shows a maximum. This different behavior should be explained from Eqs. (2.2) and (2.3). The diagonal impedance is inversely proportional to skin depth, thus when the frequency increases and δ decreases, $|Z_{zz}|$ increases. However, the off-diagonal impedance is directly proportional to $(\omega \mu_{zy} \delta)$. There is a competition between the magnetic induction term $(\omega \mu_{zy})$, which increases with the frequency, and the skin depth δ that decreases with the frequency. As a consequence the off-diagonal impedance exhibits a peak [17].

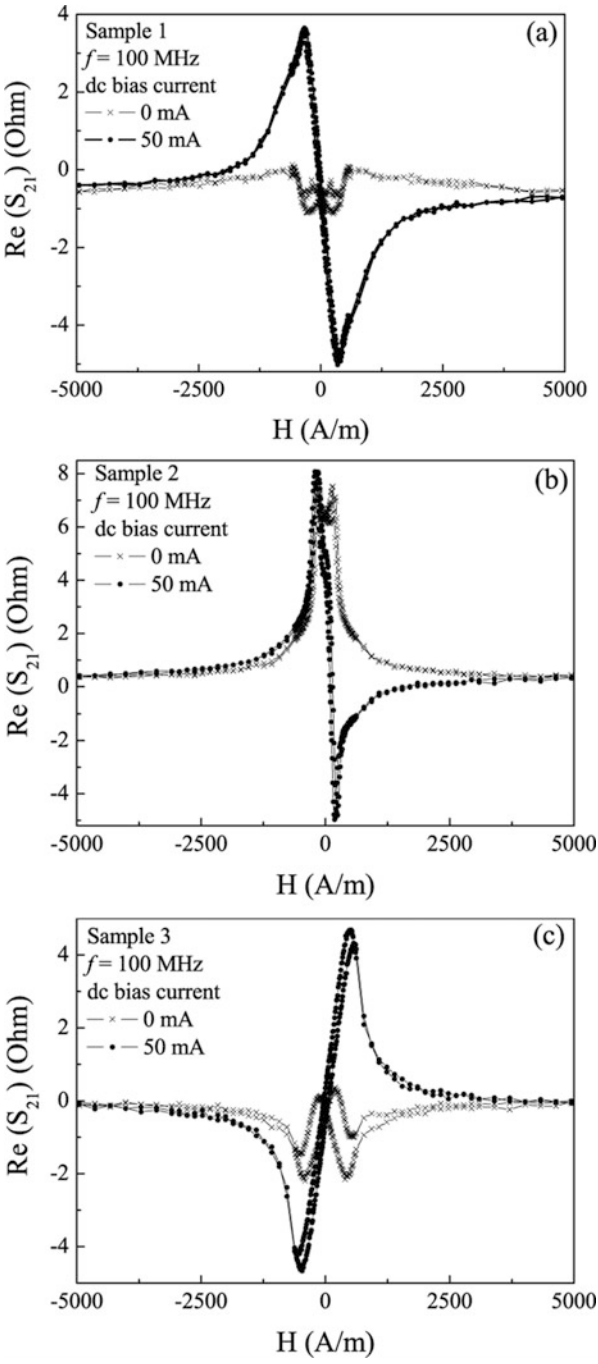

Fig. 2.9 Real part of the off-diagonal impedance (in terms of S_{21}-parameter) dependencies on external axial magnetic field with the dc bias current as a parameter at $f = 100$ MHz for (**a**) sample 1, (**b**) sample 2, and (**c**) sample 3

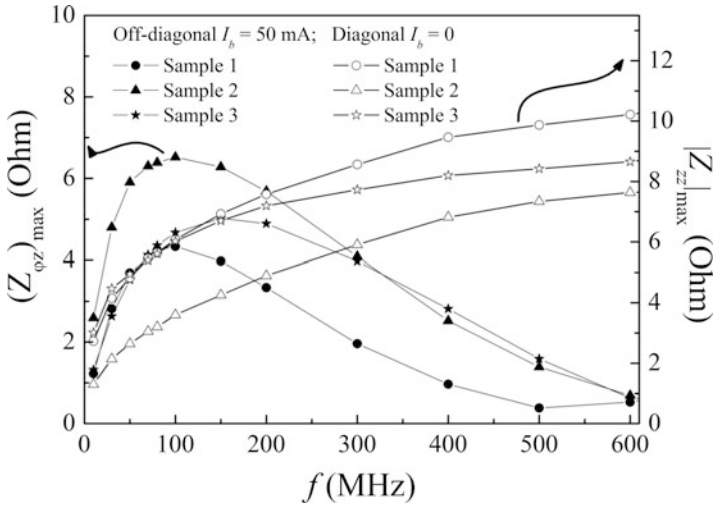

Fig. 2.10 Frequency dependence of maximum off-diagonal and diagonal impedance components for the three annealed samples. Symbols denote experimental data and lines are guides for the eye

2.5.2 *Influence of Current Annealing on GMI Effect in Co-Rich Amorphous Ribbons*

Joule annealing requires short annealing time to enhance soft magnetic behavior exhibited by Co-based nearly zero magnetostriction coefficient [45], and the references therein. To study the current-annealing effect on the longitudinal magnetoimpedance of the $Co_{71.25}Fe_{3.75}Si_{10}B_{15}$ ribbon, 1 cm long pieces of the as-quenched ribbon were Joule annealed with a dc electrical current (440–680 mA) passing during 5 min along the ribbon. This annealing process develops a transverse magnetic anisotropy of average value of around 100 J/m, although of inhomogeneous character, that enhances the transverse susceptibility [11, 46].

Figure 2.11 shows 3-D variation of the electrical giant magnetoimpedance ratio, $\Delta Z/Z(H, I_{ann})$, as a function of the applied magnetic field with the annealing current intensity, $I_{ann,}$ as a parameter, at selected frequencies between 100 and 3500 MHz of the ac electrical current flowing along the ribbon. It can be seen that a two-peaks response (symmetrically with respect to H) is present in all the frequency range for all samples. The value of H corresponding to the peaks ($\Delta Z/Z$ maximum value) is linked to the average value of the anisotropy field, H_K, at high frequency values, and to the anisotropy distribution in the sample. As it is expected, as a general rule, the evolution of $\Delta Z/Z(\%)$ with the frequency for the current-annealed ribbons shows that the maximum increases with the frequency, remaining the two-peaks behavior.

To remark the effect of current-annealing intensity on the GMI response, we have plotted the variations of $\Delta Z/Z(\%)$ as a function of I_{ann} in Fig. 2.12 at different values of the driving current frequency. As can be observed, this $\Delta Z/Z(\%)$ variation

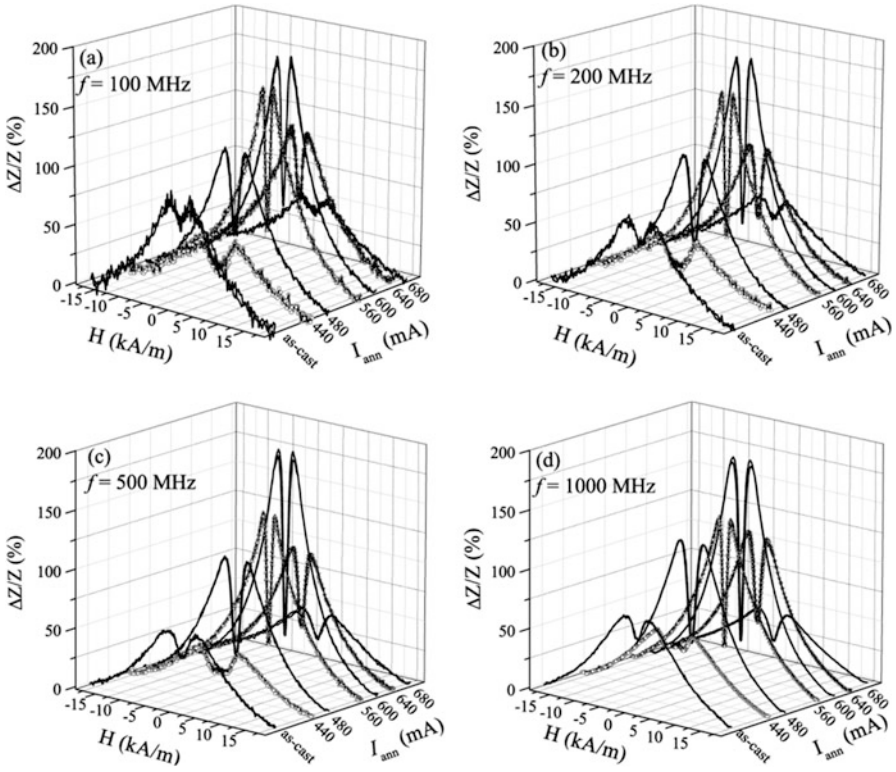

Fig. 2.11 GMI ratio as a function of the magnetic field applied along the ribbon axis at different values of the driving current frequency: (**a**) 100 MHz, (**b**) 200 MHz, (**c**) 500 MHz, and (**d**) 1000 MHz for Joule annealed $Co_{71.25}Fe_{3.75}Si_{10}B_{15}$ ribbons at different current intensities

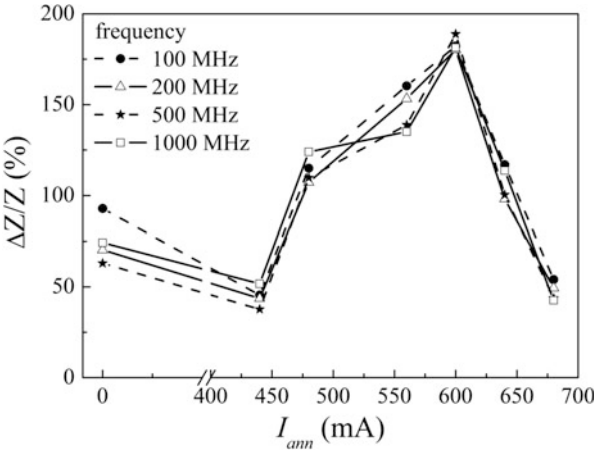

Fig. 2.12 Frequency dependence of the GMI ratio as a function of the annealing current I_{ann}. Symbols denote experimental data and lines are guides for the eye

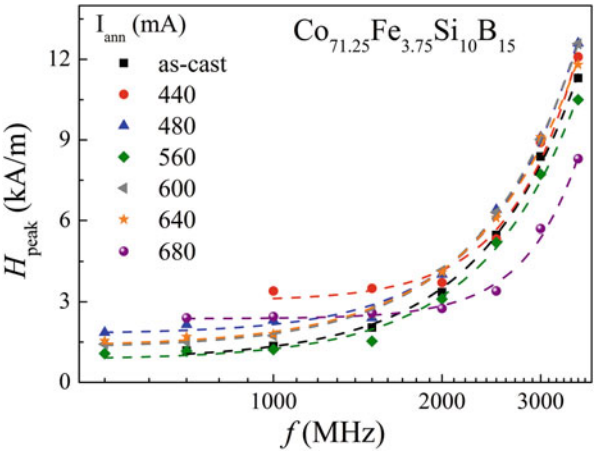

Fig. 2.13 Frequency dependence of the magnetic field, H_{peak}, where GMI ratio presents a maximum for current-annealed $Co_{71.25}Fe_{3.75}Si_{10}B_{15}$ ribbons. Symbols denote experimental data and lines are guides for the eye

presents a maximum around 600 mA, which is the intensity of current annealing to develop the maximum transverse induced magnetic anisotropy such has been reported in [37, 46].

Furthermore, the frequency dependence of the value of the magnetic field, H_{peak}, where the GMI ratio presents the maximum value, is represented in Fig. 2.13 for all as-cast and current-annealed ribbons. It can be seen that the H_{peak} value increases with the frequency for all samples.

Maximum GMI response and H_{peak} value depend on the annealing current intensity, since both features are strongly connected to the anisotropy field. The origin of the H_{peak} shift as the frequency increases is related to the change in skin depth through the frequency-dependent magnetic permeability. As increasing the driving frequency of the ac electric current along the ribbon, a decrease of the surface layer thickness is produced and transverse permeability should drastically change. The application of a longitudinal magnetic field large enough for saturating the sample modifies the transverse permeability by the reorientation of the static magnetization, and by the own permeability change simultaneously. As a consequence, the effective skin depth increases, providing an impedance decreasing.

As mentioned above, the H_{peak} value corresponding to the maximum of the magnetoimpedance of all the samples is shifted towards larger field values when the frequency is increased. This is a conclusive evidence of the ferromagnetic resonance contribution to the GMI effect [38]. Studying the position of the FMR peaks, i.e., the frequency at which appears a maximum of the impedance for each field H, we can observe that data are well fitted by the above mentioned FMR expression, Eq. (2.5), except for the Joule annealed sample with 680 mA current intensity (see Fig. 2.14).

It is worthwhile mentioning that this ribbon showed a clear trace of the first stage of crystallization as was shown in [37].

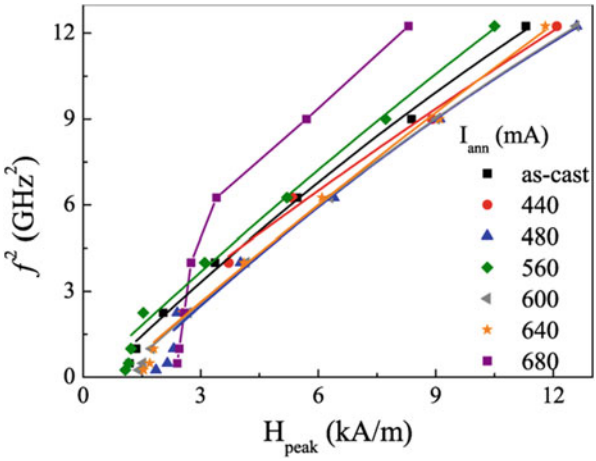

Fig. 2.14 Square of frequency as a function of H_{peak} for current-annealed $Co_{71.25}Fe_{3.75}Si_{10}B_{15}$ amorphous ribbons. Symbols denote experimental data and lines denote theoretical fits by Eq. (2.5)

2.6 Conclusions

Giant magnetoimpedance response of Co-rich amorphous $Co_{71.25}Fe_{3.75}Si_{10}B_{15}$ and $Co_{66.3}Fe_{3.7}Si_{12.0}B_{18.0}$ alloy ribbons results to be rather sensitive to current-annealing and stress-annealing treatments, respectively, as a consequence of the induction of different uniaxial anisotropy transverse to the ribbon axis, affecting drastically the soft magnetic character of the sample. Two-peaks behavior of the GMI effect is observed in all current-annealed ribbons. The effect is enhanced as increasing the intensity of the annealing current (up to 600 mA at which $\Delta Z/Z$ ratio achieves its maximum value). This behavior is explained in terms of the frequency dependence of skin depth and the dispersion of easy axes through the ribbon thickness. Moreover, the macroscopic magnetic anisotropy induced by this thermal treatment has an inhomogeneous character as a consequence of the non-uniform transverse field created by the electric current through the ribbon cross section during the annealing. In the case of stress-annealing ribbons, the GMI response is sharper and narrower as a consequence of the more uniform induced anisotropy in comparison with the as-quenched ribbon, which has to be considered as key-factor for sensing applications. Two-peaks behavior in the GMI effect is observed for the ribbon stress annealed at 400 °C, while in those samples submitted to a previous stress relaxation the two-peaks behavior show some peculiarities. The ribbon pre-annealed at 340 °C displays two-peaks behavior but emerging at frequency above 150 MHz, while the sample pre-annealed at 360 °C shows an asymmetry in the GMI effect. Finally, ferromagnetic resonance effects at high frequencies are detected in all studied ribbons.

Acknowledgements This work was financially supported by the Spanish MINECO Ref. MAT2013-47231-C2-1-P, Ref. MAT2013-47231-C2-2-P, and Ref. MAT2013-48054-C2-2-R, Asturias Government Ref. FC-15-GRUPIN14-085, Basque Government under Saiotek 13 PROMAGMI (SPE13UN014), and DURADMAG (S-PE13UN007). Technical and human support provided by SGIker (UPV/EHU, MICINN, GV/EJ, ERDF, and ESF) is gratefully acknowledged.

References

1. Jiles, D.C.: Recent advances and future directions in magnetic materials. Acta Mater. **51**, 5907 (2003)
2. Hasegawa, R.: Advances in amorphous and nanostructured materials. J. Optoelectron. Adv. Mater. **6**, 503 (2004)
3. Zhukov, A., Ipatov, M., Churyukanova, M., Kaloshkin, S., Zhukova, V.: Giant magnetoimpedance in thin amorphous wires: from manipulation of magnetic field dependence to industrial applications. J. Alloys Compd. **586**, S279 (2014)
4. Panina, L.V., Mohri, K.: Magneto-impedance effect in amorphous wires. Appl. Phys. Lett. **65**, 1189 (1994)
5. Beach, R., Berkowitz, A.: Giant magnetic field dependent impedance of amorphous FeCoSiB wire. Appl. Phys. Lett. **64**, 3652 (1994)
6. Honkura, Y.: Development of amorphous wire type MI sensors for automobile use. J. Magn. Magn. Mater. **249**, 375 (2002)
7. Mohri, K., Uchiyama, T., Shen, L.P., Cai, C.M., Panina, L.V.: Amorphous wire and CMOS IC-based sensitive micro-magnetic sensors (MI sensor and SI sensor) for intelligent measurements and controls. J. Magn. Magn. Mater. **249**, 351 (2002)
8. Marín, P., López, M., Vlad, A., Hernando, A., Ruiz-González, M.L., González-Calbet, J.M.: Magnetic field driving custom assembly in (FeCo) nanocrystals. Appl. Phys. Lett. **89**, 033508 (2006)
9. Ohodnicki, P.R., Laughlin, D.E., McHenry, M.E., Keylin, V., Huth, J.: Temperature stability of field induced anisotropy in soft ferromagnetic Fe, Co-based amorphous and nanocomposite ribbons. J. Appl. Phys. **105**, 07A322 (2009)
10. Chaturvedi, A., Laurita, N., Leary, A., Phan, M.-H., McHenry, M.E., Srikanth, H.: Giant magnetoimpedance and field sensitivity in amorphous and nanocrystalline $(Co_{1-x}Fe_x)_{89}Zr_7B_4$ (x = 0, 0.025, 0.05, 0.1) ribbons. J. Appl. Phys. **109**, 07B508 (2011)
11. Laurita, N., Chaturvedi, A., Bauer, C., Jayathilaka, P., Leary, A., Miller, C., Phan, M.-H., McHenry, M.E., Srikanth, H.: J. Appl. Phys. **109**, 07C706 (2011)
12. Manna, S.K., Srinivas, V.: Magnetic and magnetoimpedance studies on controlled Joule annealed amorphous $Co_{73}Fe_{4.5}Ni_{0.5}Mn_{0.5}Nb_{0.5}Si_{4.2}B_{16.8}$ alloy. J. Appl. Phys. **115**, 17A324 (2014)
13. Knobel, M., Vazquez, M., Kraus, L.: Giant magnetoimpedance. In: Buschow, K. (ed.) Handbook of Magnetic Materials, pp. 497–563. Elsevier, North-Holland (2003)
14. Phan, M.-H., Peng, H.-X.: Giant magnetoimpedance materials: fundamentals and applications. Prog. Mater. Sci. **53**, 323 (2008)
15. Kraus, L.: Theory of giant magneto-impedance in the planar conductor with uniaxial magnetic anisotropy. J. Magn. Magn. Mater. **195**, 764 (1999)
16. Makhnovskiy, D.P., Panina, L.V., Mapps, D.: Field-dependent surface impedance tensor in amorphous wires with two types of magnetic anisotropy: helical and circumferential. Phys. Rev. B. **63**, 144424-1–144424-17 (2001)
17. Kraus, L.: Off-diagonal magnetoimpedance in stress-annealed amorphous ribbons. J. Magn. Magn. Mater. **320**, e746–e749 (2008)
18. Kraus, L., Vázquez, M., Infante, G., Badini-Confalonieri, G., Torrejón, J.: Nonlinear magnetoimpedance and parametric excitation of standing spin waves in a glass-covered microwave. Appl. Phys. Lett. **94**, 062505 (2009)
19. Panina, L.V., Mohri, K., Uchiyama, T., Noda, M., Bushida, K.: Giant magneto-impedance in Co-rich amorphous wires and films. IEEE Trans. Magn. **31**, 1249 (1995)
20. Ciureanu, P., Britel, M., Ménard, D., Akyel, C., Yelon, A., Rouabhi, M., Cochrane, R.W.: Anisotropic behavior of permalloy wires using the giant magnetoimpedance effect. J. Magn. Magn. Mater. **196–197**, 391 (1999)
21. Crisan, O., Le Breton, J.M., Filoti, G.: Nanocrystallization of soft magnetic Finemet-type amorphous ribbons. Sens. Actuators A. **106**, 246 (2003)

22. Zhang, K., Zhou, D.W., Han, B., Lv, Z., Xun, X.C., Du, X.B., Liu, Y.Q., Yao, B., Zhang, T., Li, B.H., Wang, D.: Annealing temperature dependence of magnetic properties and magneto-impedance effect in CoZrB alloys. J. Alloys Compd. **464**(28), (2008)
23. Allia, P., Tiberto, P., Baricco, M., Vinai, F.: dc Joule annealing of amorphous metallic ribbons: experimental aspects and model. Rev. Sci. Instrum. **64**, 1053 (1993)
24. Sahoo, T., Majundar, B., Srivinas, V., Srinivas, M., Nath, T.K., Agarwal, G.: Improved magnetoimpedance and mechanical properties on nanocrystallization of amorpous $Fe_{68.5}Si_{18.5}Cu_1Nb_3B_9$ ribbons. J. Magn. Magn. Mater. **343**, 13 (2013)
25. Hoque, S.M., Haque, A., Rahman, M.O., Nghi, N.H., Hakim, M.A., Akther, S.: Ultra-soft magnetic properties and giant magneto-impedance of $Co_{68}Fe_{4.5}Si_{12.5}B_{15}$. J. Non-Cryst. Solids. **357**, 2109 (2011)
26. Kotagiri, G., Ramarao, S.D., Markandeyulu, G.: Magnetoimpedance studies on laser and microwave annealed $Fe_{66}Ni_7Si_7B_{20}$ ribbons. J. Magn. Magn. Mater. **382**, 43 (2015)
27. González, L., Bonastre, J., Sánchez, T., Santos, J.D., Sánchez, M.L., Chiznik, A., Domínguez, L., Ipatov, M., Zhukova, V., Zhukov, A., González, J., Suñol, J.J., Hernando, B.: Magnetoimpedance response in Co-based amorphous ribbons obtained under the action of a magnetic field. IEEE Trans. Magn. **48**, 4375 (2012)
28. Kim, C.G., Jang, K.J., Kim, H.C.: Asymmetric giant magnetoimpedance in field-annealed Co-based amorphous ribbon. J. Appl. Phys. **15**, 5447–5449 (1999)
29. Gupta, P., Gupta, A., Franco, V., Conde, A.: Joule heating as a technique for obtaining uncoupled soft and hard magnetic phases in a Finemet alloy. J. Appl. Phys. **101**, 133909 (2007)
30. Shari, F., Beitollahi, A., Shabestari, S.G., Ghanaatshoar, M., Tehranchi, M.M., Mohseni, S.M., Roozmeh, S.E., Wanderka, N., Florillo, F.: Structural characterization and magnetoimpedance effect in amorphous and nanocrystalline Al Ge-substituted FeSiBNbCu ribbons. J. Magn. Magn. Mater. **312**, 35–42 (2007)
31. Bonastre, J., Suñol, J.J., Bruna, P., Sato, K., Santos, J.D., Hernando, B.: Influence of a magnetic field applied during the quenching process on the spin density and nanoscale of an amorphous Fe-B ribbon. Mater. Lett. **87**, 131–134 (2012)
32. Talaat, A., Ipatov, M., Zhukova, V., Zhukov, A.P., González, J., González-Legarreta, L., Prida, V.M., Hernando, B.: High frequency magnetoimpedance response of stress annealed $Co_{66.3}Fe_{3.7}Si_{12.0}B_{18.0}$ amorphous alloy ribbons. J. Appl. Phys. **114**, 023904 (2013)
33. Narita, K., Yamasaki, J., Fukunaga, H.: Measurement of saturation magnetostriction of a thin amorphous ribbon by means of small-angle-magnetization-rotation. IEEE Trans. Magn. **16**, 435 (1980)
34. Ipatov, M., Zhukova, V., Zhukov, A., González, J.: Expanding the longitudinal magnetoimpedance sensor range by direct bias current. J. Appl. Phys. **113**, 203902 (2013)
35. Nielsen, O.V.: Effects of longitudinal and torsional stress annealing on the magnetic anisotropy in amorphous ribbon materials. IEEE Trans. Magn. **21**, 2008 (1985)
36. Blanco, J.M., Barbón, P.G., Pierna, A.R., González, J.: Compositional dependence of the stress plus field induced anisotropy in Co-Ni-Si-B and Co-Fe-Ni-Si-B amorphous alloy ribbons. J. Non-Cryst. Solids. **136**, 91 (1991)
37. Vázquez, M., González, J., Hernando, A.: Induced magnetic anisotropy and change of the magnetostriction by current annealing in Co-based amorphous alloys. J. Magn. Magn. Mater. **53**, 323 (1986)
38. Barandiarán, J.M., García-Arribas, A., de Cos, D.: Transition from quasistatic to ferromagnetic resonance regime in giant magnetoimpedance. J. Appl. Phys. **99**, 103904 (2006)
39. Antonov, A.S., Iakubov, I.A., Lagarikov, A.N.: Longitudinal-transverse linear transformation of the HF-current in soft magnetic materials with induced anisotropy. IEEE Trans. Magn. **33**, 3367 (1997)
40. Buznikov, N.A., Kim, C.G., Kim, C.O., Yoon, S.S.: Asymmetric off-diagonal magnetoimpedance in field-annealed amorphous ribbons: analysis of bias current effect. J. Magn. Magn. Mater. **309**, 216 (2007)

41. Malátek, M., Kraus, L.: Off-diagonal GMI sensor with stress-annealed amorphous ribbon. Sens. Actuators A. **164**, 41–45 (2010)
42. Ipatov, M., Zhukova, V., Zhukov, A., Gonzalez, J., Zvezdin, A.: Low field hysteresis in the magnetoimpedance of amorphous microwires. Phys. Rev. B. **81**, 134421 (2010)
43. Ipatov, M., Zhukova, V., Zhukov, A., Gonzalez, J.: Magnetoimpedance sensitive to dc bias current in amorphous microwires. Appl. Phys. Lett. **97**, 252507 (2010)
44. Ipatov, M., Zhukova, V., Gonzalez, J., Zhukov, A.: Symmetry breaking effect of dc bias current on magnetoimpedance in microwire with helical anisotropy: application to magnetic sensors. J. Appl. Phys. **110**, 086105 (2011)
45. Manna, S.K., Srinivas, V.: Magnetic and magnetoimpedance studies on controlled Joule annealed amorphous $Co_{73}Fe_{4.5}Ni_{0.5}Mn_{0.5}Nb_{0.5}Si_{4.2}B_{16.8}$ alloy. J. Appl. Phys. **115**, 17A324 (2011)
46. Ipatov, M., González-Legarreta, L., Garcia, J., Chizhik, A., Domínguez, L., Zhukova, V., Zhukov, A., Hernando, B., González, J.: Induced giant magnetoimpedance effect by current annealing in ultra thin Co-based amorphous ribbons. IEEE Trans. Magn. **49**, 1009 (2012)